Pramana – J. Phys. (2021) 95:106
https://doi.org/10.1007/s12043-021-02146-5

Deep sub-barrier breakup dynamics in the ^{8}B + ^{208}Pb reaction

B MUKERU*, L V NDALA and M L LEKALA

Department of Physics, University of South Africa, P.O. Box 392, Pretoria 0003, South Africa
*Corresponding author. E-mail: mukerb1@unisa.ac.za

MS received 5 December 2020; revised 18 February 2021; accepted 12 March 2021

Abstract. Breakup reactions at deep sub-barrier incident energies are the less investigated in the breakup of loosely-bound systems. Motivated by a recent study by Pakou *et al* (*Phys. Rev. C* **102**:031601(R), 2020), we further analyse the breakup of ^{8}B nucleus on a lead target at deep sub-barrier incident energies. It is found that at these energies, continuum–continuum couplings enhance the breakup cross-section. These couplings are otherwise known to hinder the breakup cross-section at energies around and above the Coulomb barrier. We argue that this enhancement can in part explain the known predominance of the breakup channel over other reaction channels at deep sub-barrier energies, and that it may signal a breakup on the outgoing trajectory. The results in this paper also confirm the prediction in the reference above. Due to the astrophysical aspect of ^{8}B nucleus, this result could have significant implication in nuclear astrophysics.

Keywords. Breakup reaction; breakup cross-section; continuum–continuum couplings; deep sub-barrier energies.

PACS Nos 12.60.Jv; 12.10.Dm; 98.80.Cq; 11.30.Hv

1. Introduction

Since the early works such as in ref. [1], the study of nuclear halos and other loosely bound systems has attracted immense attention to become one of the hottest subjects in the nuclear physics community (see for example refs [2–6], for some of the recent reviews on this subject). Due to their low breakup threshold, the breakup process is regarded as the most adequate tool to probe the structure of these nuclei, making the breakup effect on other reaction channels, such as fusion, elastic scattering, etc., one of the most documented topics in the subject. Although breakup reactions have been extensively investigated at incident energies around and above the Coulomb barrier, this is not the case at deep sub-barrier energies, which is the energy region of nuclear astrophysics interest.

For example, while it is well understood that the continuum–continuum couplings strongly suppress/hinder the breakup cross-section, as evidenced, for example by refs [7–10], at deep sub-barrier energies, it is shown in ref. [11], that these couplings rather enhance the breakup cross-section, in the breakup of ^{6}Li nucleus on different target masses. If this conclusion can be extended to other loosely bound systems, it could pave the way towards a better understanding of the importance of the breakup process in nuclear astrophysics. Also, at deep sub-barrier incident energies, the breakup process has been shown to be the main reaction channel as the breakup cross-section is reported to account for almost the whole reaction cross-sections (see for example refs [5,12], and references therein). This result has also been confirmed in ref. [13], where the breakup cross-section in the ^{8}B + ^{208}Pb reaction was measured for the first time at $E_{\rm lab} = 30$ MeV. However, the reaction dynamics leading to the predominance of the breakup channel at deep sub-barrier energies are not fully elucidated. The interest in the ^{8}B nucleus at such low incident energy, not only stems from the fact that it is the lightest proton-halo nucleus, but also due to its potential role in the production of high-energy neutrinos in the Sun [14,15]. Therefore, the study of its breakup at deep sub-barrier energies could have a significant astrophysical implication.

Another outstanding issue as far as the breakup effect is concerned, is the origin of the complete fusion suppression. This suppression is generally believed to be dependent on the projectile breakup threshold (more discussion on complete fusion can be found in ref. [3], and references therein). However, recent

Published online: 21 June 2021

studies such as in refs [16–20], are suggesting other reaction mechanisms as the main source of complete fusion suppression. Recent measurements of the complete fusion cross-section in ^{7,8}Li + ^{209}Bi reactions in refs [16,17] concluded that a charge clustering rather than a weak projectile binding is the main factor that contributes to the complete fusion suppression. It is also argued in refs [18–20] that the complete fusion suppression cannot be fully explained by breakup prior to reaching the fusion barrier. In ref. [19], it is predicted that for light target a sizeable complete fusion suppression is unlikely for ^{6,7}Li projectiles at incident energies above the Coulomb barrier, although the underlying reaction dynamics remain to be exposed.

In refs [21,22] (and references therein), the complete fusion suppression is attributed to couplings to resonant states with long half-lives, which reduce the probability of a breakup prior to reaching the fusion barrier. Other studies, such as in refs [23–26], have also reported a significant effect of the projectile resonances on elastic scattering and breakup cross-sections. Although the delay in the breakup process is well associated with couplings to resonant states, one would expect continuum–continuum couplings whether between resonant or non-resonant states to produce the same effect, albeit with a different magnitude. Being multistep processes, couplings between continuum states can be expected to delay the breakup process compared to couplings to and from the ground state, which represent a single process.

In fact, in ref. [27], it is found that fusion dynamics strongly depend on the continuum–continuum couplings. In order to better assess the effect of non-resonant continuum–continuum couplings on the complete fusion cross-section, one would need to consider a projectile without any continuum structure (i.e. no resonances).

Motivated by the recent experimental study in ref. [13], in this paper, we propose to study the ^{8}B + ^{208}Pb breakup reaction at deep sub-barrier, around, and above the Coulomb barrier incident energies. To this end, we investigate whether or not the continuum–continuum couplings enhance the breakup and complete fusion cross-sections at deep sub-barrier energies as reported in ref. [11]. We believe that this study may lead to a better understanding of the predominance of the breakup channel at deep sub-barrier energies. We will also compare the breakup, total reaction and total fusion cross-sections in an effort to provide further theoretical support to the conclusions of ref. [13]. As in refs [9,11,27,28], we shall also investigate the continuum–continuum coupling effect on the complete fusion cross-section, which may be crucial towards a better understanding of the origin of the complete fusion.

The paper is organised as follows: In §1, a brief theoretical description is presented, the details of the numerical calculations are given in §3, the results are presented and discussed in §4, whereas the conclusions are reported in §5.

2. Brief theoretical consideration

As in any other coupled-channels formalism, in the CDCC formalism [29,30], which is the theoretical approach adopted in this work, once the total wave function has been expanded on a complete basis of the projectile internal states, the following set of coupled differential equations is obtained:

$$\left\{\frac{\hbar^2}{2\mu_{pt}}\left[\frac{\mathrm{d}^2}{\mathrm{d}R^2}-\frac{L(L+1)}{R^2}\right]+\mathscr{U}^{LJ}_{\alpha\alpha}(R)+\varepsilon_\alpha-E\right\}\mathscr{F}^{LJ}_{\alpha}(R)+\sum_{\alpha\neq\alpha'}\mathscr{U}^{LL'J}_{\alpha\alpha'}(R)\mathscr{F}^{L'J}_{\alpha'}(R)=0, \tag{1}$$

where μ_{pt} is the projectile–target reduced mass, $\alpha \equiv (\alpha_b, \alpha_{\alpha_i})$, with $\alpha_b = \{\ell_b, s, j, I, \tilde{j}_b\}$ and $\alpha_i = \{i, \ell, s, j, I, \tilde{j}\}$ ($i = 1, 2, \ldots, N_b$, with N_b being the number of bins), are sets of quantum numbers that describe the projectile bound and continuum states, respectively (ℓ_b is the orbital angular momentum in the projectile ground state, I and s are the core and valence nucleon spins, respectively and ℓ is the orbital angular momentum in the projectile continuum. The total angular momenta $\tilde{j}_b$ in the ground state and $\tilde{j}$ in the continuum, are obtained through the following coupling schemes: $\boldsymbol{\ell}_b(\boldsymbol{\ell}) + \boldsymbol{s} = \boldsymbol{j}_b(\boldsymbol{j})$, $\boldsymbol{j}_b(\boldsymbol{j}) + \boldsymbol{I} = \tilde{\boldsymbol{j}}_b(\tilde{\boldsymbol{j}})$), $\varepsilon_\alpha = \{\varepsilon_b, \varepsilon_{\alpha_i}\}$, with $\varepsilon_b < 0$, the ground-state binding energy, and ε_{α_i} being the bin energies. In this equation, $\mathscr{F}^{LJ}_{\alpha}(R)$ is the projectile–target radial wave function, with L, the orbital angular momentum associated with the centre-of-mass coordinate R, and $J = \tilde{j} + L$, the total angular momentum of the system. The different channels are coupled by the coupling matrix elements $\mathscr{U}^{LL'J}_{\alpha\alpha'}(R)$, which are given by

$$\mathscr{U}^{LL'J}_{\alpha\alpha'}(R) = \langle \mathscr{Y}^{LJ}_{\alpha}(\boldsymbol{r}, \Omega_{\boldsymbol{R}}) | U_{pt}(\boldsymbol{r}, \boldsymbol{R}) | \mathscr{Y}^{L'J}_{\alpha'}(\boldsymbol{r}, \Omega_{\boldsymbol{R}}) \rangle, \tag{2}$$

where $U_{pt}(\boldsymbol{r}, \boldsymbol{R})$ is the projectile–target potential, being a sum of the core–target [$U_{ct}(\boldsymbol{R}_{ct})$], and nucleon–target

$[U_{vt}(\boldsymbol{R}_{vt})]$ optical potentials, with

$$\boldsymbol{R}_{ct} = \boldsymbol{R} + \frac{A_v}{A_p}\boldsymbol{r}$$

and

$$\boldsymbol{R}_{vt} = \boldsymbol{R} - \frac{A_c}{A_p}\boldsymbol{r},$$

the core and valence nucleon coordinates, where A_c, A_v and $A_p = A_c + A_v$, are respectively the core, valence nucleon and projectile atomic mass numbers. The channel wave function $\mathscr{Y}_{\alpha}^{LJ}(\boldsymbol{r}, \Omega_{\boldsymbol{R}})$, where $\Omega_{\boldsymbol{R}} \equiv (\theta, \phi)$ is the solid angle in the direction of the coordinate R, contains square-integrable bound and continuum bin wave functions of the projectile. These matrix elements can be split as follows:

$$\mathscr{U}_{\alpha\alpha'}^{LL'J}(R) = \langle \mathscr{Y}_{\alpha_b}^{LJ}(\boldsymbol{r}, \Omega_{\boldsymbol{R}}) | U_{pt}(\boldsymbol{r}, \boldsymbol{R}) | \mathscr{Y}_{\alpha_i}^{LJ}(\boldsymbol{r}, \Omega_{\boldsymbol{R}}) \rangle + \langle \mathscr{Y}_{\alpha_i}^{LJ}(\boldsymbol{r}, \Omega_{\boldsymbol{R}}) | U_{pt}(\boldsymbol{r}, \boldsymbol{R}) | \mathscr{Y}_{\alpha_i'}^{L'J}(\boldsymbol{r}, \Omega_{\boldsymbol{R}}) \rangle, \tag{3}$$

where the first term represents couplings to and from the ground state and the second term stands for the continuum–continuum couplings.

Once the different coupling matrix elements have been evaluated after an expansion of the projectile–target potential into potential multipoles (see for instance ref. [31] for more details), the coupled equations (1) are numerically solved with the usual boundary conditions in the asymptotic region

$$\mathscr{F}_{\alpha}^{LJ}(R) \overset{R\to\infty}{\to} \frac{i}{2}\left[H_L^-(K_\alpha R)\delta_{\alpha\alpha'} - H_L^+(K_\alpha R) S_{\alpha\alpha'}^J(K_\alpha)\right], \tag{4}$$

where $H_L^{\pm}(K_\alpha R)$ are Coulomb–Hankel functions [32] and $S_{\alpha\alpha'}^J(K_\alpha)$ is the S-matrix [$S_{\alpha\alpha'} \equiv (S_{\alpha_b\alpha_b}, S_{\alpha_i\alpha_i'})$ with $S_{\alpha_b\alpha_b}$ and $S_{\alpha_i\alpha_i'}$ being the elastic scattering and breakup S-matrices, respectively], $K_\alpha \equiv (K_{\alpha_b}, K_{\alpha_i})$, with

$$K_{\alpha_b} = \sqrt{\frac{2\mu_{pt}(E - \varepsilon_b)}{\hbar^2}}$$

and

$$K_{\alpha_i} = \sqrt{\frac{2\mu_{pt}(E - \varepsilon_{\alpha_i})}{\hbar^2}},$$

being the wave numbers in the elastic and breakup channels. Various breakup observables can be obtained from the breakup S-matrix, as outlined in refs [32,33]. The total and complete fusion cross-sections can be obtained from the full wave function $\mathscr{F}_{\alpha}^{LJ}(R)$, as discussed in refs [27,31,34,35], where the complete fusion is defined as an absorption from the bound states [27].

3. Details of numerical calculations

The projectile nucleus ^{8}B is modelled as $^8\mathrm{B} \to {}^7\mathrm{Be} + p$, with an experimental ground-state binding energy $\varepsilon_b = 0.137$ MeV [36], with quantum numbers $\ell_b = 1$ and $\tilde{j}_b^{\pi} = 2^+$. This state is obtained by coupling the proton in the $0p_{3/2}$ orbit with the $\frac{3}{2}^-$ ground-state of ^{7}Be core nucleus. The parameters of the Woods–Saxon potential used to calculate bound-state and continuum wave functions, taken from ref. [37], are: $V_0 = -44.65$ MeV, $V_{\mathrm{so}} = -19.59$ MeV $\cdot$ fm^2, $a_0 = a_{\mathrm{so}} = 0.52$ fm and $R_0 = R_{\mathrm{so}} = R_{\mathrm{C}} = 2.391$ fm, where V_0 and V_{so} are the depths of the central and spin–orbit coupling terms of the nuclear component, with R_0, R_{so} and a_0, a_{so}, the corresponding radii and diffuseness, respectively and R_{C} is the Coulomb radius. The parameter V_0 was adjusted to obtain the other binding energy $\varepsilon_b = 1.0$ MeV, which is also considered in this work. As in ref. [13], we adopted the parameters of the ^{6}Li global potential [38] for the $^7\mathrm{Be} + {}^{208}\mathrm{Pb}$ potential, whereas the $p + {}^{208}\mathrm{Pb}$ potential parameters were taken from ref. [39].

The numerical parameters used to integrate the coupled differential equations (1) were determined as follows: the maximum angular momentum between the ^{7}Be core nucleus and the proton was truncated by $\ell_{\max} = 4\hbar$, for $E_{\mathrm{c.m.}}/V_{\mathrm{B}} < 1.0$ and by $\ell_{\max} = 5\hbar$ for $E_{\mathrm{c.m.}}/V_{\mathrm{B}} \geq 1.0$ (where $V_{\mathrm{B}} = 49.36$ MeV is the Coulomb barrier height, calculated with the São Paulo potential (SPP) [40]). The maximum matching radius for bin integration was truncated by $r_{\max} = 100$ fm, the maximum order of the potential multipole expansion, by $\lambda_{\max} = 5$, the maximum matching radius of the integration of the coupled differential equations by $R_{\max} = 1000$ fm, the maximum angular momentum of the relative centre-of-mass motion, by $L_{\max} = 1000\hbar$ and the ^{7}Be-proton maximum relative momentum, by $k_{\max} = 0.6$ fm^{-1}, for $E_{\mathrm{c.m.}}/V_{\mathrm{B}} < 1.0$ and by $k_{\max} = 1.0$ fm^{-1}, for $E_{\mathrm{c.m.}}/V_{\mathrm{B}} \geq 1.0$. The interval $[0, k_{\max}]$ was then sliced into momentum bins of widths, $\Delta k = 0.1$ fm^{-1}, for s- and p-states, $\Delta k = 0.2$ fm^{-1}, for f- and d-states and $\Delta k = 0.25$ fm^{-1}, for higher-order partial waves. The numerical calculations were carried out with Fresco code [32].

4. Results and discussion

The integrated breakup cross-sections obtained when all the different couplings are included ('All coupl.') and when the continuum–continuum couplings ('No ccc') are excluded from the coupling matrix elements are shown in figure 1a, as functions of the centre-of-mass incident energy, in the range $0.4 \leq E_{\mathrm{c.m.}}/V_{\mathrm{B}} \leq$

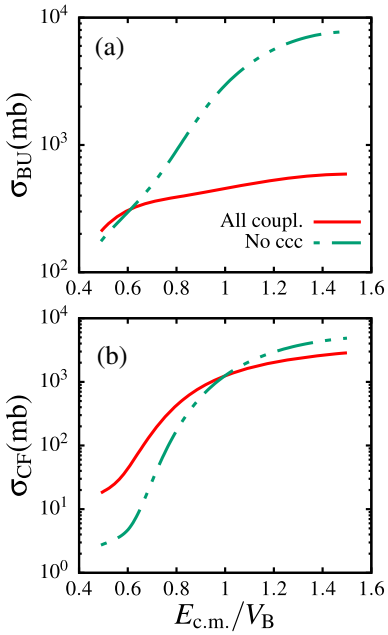

Figure 1. Integrated breakup (**a**) and complete fusion (**b**) cross-sections for different centre-of-mass incident energies scaled by the Coulomb barrier height, in the presence and absence of continuum–continuum couplings.

1.5. Looking at this figure, we observe that at deep sub-barrier incident energies ($E_{c.m.}/V_B \leq 0.6$), the continuum–continuum couplings indeed enhance the breakup cross-section, whereas at $E_{c.m.}/V_B > 0.6$, the usual substantial suppression due to these couplings is displayed. This indicates that continuum–continuum couplings exhibit opposite effect at deep sub-barrier compared to their effect around and above the barrier. The similarities of these results with the ones obtained in ref. [11], in the same incident energy range, for the ^{6}Li + ^{208}Pb reaction, where the ^{6}Li projectile contains three resonances in the $\ell = 2$ partial wave, is an indication that this observation can be extended to other loosely-bound systems, regardless of whether or not they contain resonances.

Notice that the probability of the projectile breaking up on its outgoing trajectory or entering the absorption region as a bound system, is higher at deep sub-barrier energies, which is further facilitated by multistep continuum–continuum couplings, which are known to delay the breakup process. Also, it is known that these couplings enhance the irreversibility of breakup and thus reduce the flux that penetrates the Coulomb barrier [27]. If the projectile penetrates the absorption region as the bound system, there is a strong projectile–target Coulomb repulsion in the diagonal channel, which subsequently leads to a large Coulomb breakup due to the resulting weak nuclear absorption. This assertion is supported by the results of ref. [13], where the Coulomb and total breakup cross-sections are similar (see figure 3 of that reference). However, as the absence of continuum–continuum couplings leads to a more prompt breakup, in this case, the probability of the projectile entering the absorption region as a bound system is low, compared to the case where these couplings are included, which in the end weakens the projectile–target diagonal Coulomb repulsion at deep sub-barrier energies. This enhances the nuclear absorption by adding more flux from the breakup channel to the fusion channel. Therefore, one may argue that this dynamical effect can in part explain the enhancement of the breakup cross-section at deep sub-barrier energies, due to the continuum–continuum couplings. Also, this enhancement might be associated with a projectile breakup on the outgoing trajectory. Furthermore, these results suggest that at deep sub-barrier energies, the continuum–continuum couplings may relatively increase the half-life of the bound state inside the absorption region. In this case, one can also conclude that the breakup prior to reaching the Coulomb barrier cannot explain the enhancement of the breakup cross-section due to the continuum–continuum couplings.

Let us now consider the complete fusion cross-section, which is shown in figure 1b, in the presence and absence of continuum–continuum couplings. Inspecting this figure, it is noticed that couplings among continuum states strongly enhance the complete fusion cross-section at incident energies below and around the Coulomb barrier ($E_{c.m.}/V_B \simeq 1.0$), as also observed in ref. [27]. As the complete fusion cross-section depends on the bound state, it implies that the longer the projectile remains in a bound state inside the fusion barrier, the more it contributes to the complete fusion cross-section, i.e., enhancement. These results may further imply that the continuum–continuum couplings may increase the half-life of the bound state inside the fusion barrier. It could also be that more flux that contributes to the complete fusion in this incident energy region is captured as the unbroken projectile leaves the target inside the Coulomb barrier, where the nuclear absorption is less opposed by the Coulomb repulsion. On its incoming trajectory, the projectile is strongly repelled by the target, while it is accelerated on its outgoing trajectory. The nuclear absorption on the other hand, would act the same way on both trajectories. Following the same argument as in refs [18–20], we also believe that a breakup outside the Coulomb barrier cannot explain the enhancement of the complete fusion cross-section at deep sub-barrier energies. The reaction dynamics above the Coulomb barrier are quite different, where we also observe a complete fusion suppression due to continuum–continuum couplings, as reported in other works such as refs [11,27]. In this energy region, the probability of an asymptotic breakup on the projectile

incoming trajectory is high, meaning that the projectile is less likely to reach the absorption region unbroken. Therefore, the location of the breakup events on the incoming trajectory is crucial in understanding the suppression of the complete fusion, as suggested in refs [18–20].

A less prompt breakup can be further stimulated by artificially increasing the projectile ground-state binding energy. This ensures that breakup process occurs on the outgoing trajectory at deep sub-barrier incident energies. To this end, in order to obtain more insights into the conclusions above, we artificially increased the projectile ground-state binding energy from $\varepsilon_b = 0.137$ MeV to 1.0 MeV. Indeed, as one can notice in figure 2a, the breakup cross-section at deep sub-barrier energies is now strongly enhanced compared to the case of the lower binding energy in figure 1a. This appears to suggest that the enhancement of the breakup cross-section owing to the continuum–continuum couplings at deep sub-barrier energies, may be an indication of the projectile breaking up on its outgoing trajectory. More investigation into this assertion would be interesting. In figure 2b, we also notice a larger enhancement of the complete fusion cross-section, where the transition from enhancement to suppression observed in figure 1b, above the Coulomb barrier does no longer occur.

In ref. [13], where the elastic breakup cross-section of the reaction under study was measured at $E_{\rm lab} = 30$ MeV, an experimental value $\sigma_{\rm BU} = 326 \pm 84$ mb is reported. In our theoretical calculations, we obtained 317 mb, which indicates an excellent agreement with the data.

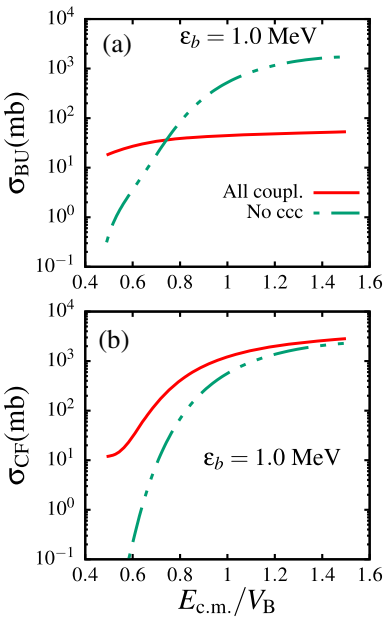

Figure 2. Integrated breakup (**a**) and complete fusion (**b**) cross-sections for different centre-of-mass incident energies scaled by the Coulomb barrier height in the presence and absence of continuum–continuum couplings, for the ground-state binding energy $\varepsilon_b = 1.0$ MeV.

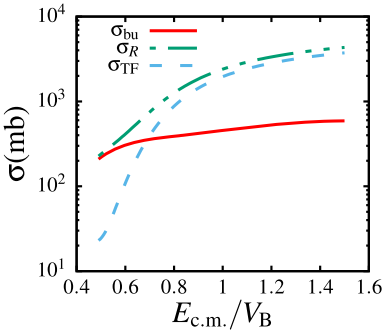

Figure 3. Total reaction, total fusion and breakup cross-sections as functions of $E_{\rm c.m.}/V_{\rm B}$.

Another important result confirmed in ref. [13] is the predominance of the breakup channel, where the breakup cross-section is reported to exhaust the total reaction cross-section, i.e., $\sigma_{\rm BU}/\sigma_R \simeq 1.0$. To verify this conclusion, we show in figure 3, the total reaction, total fusion and breakup cross-sections. We notice in this figure that in fact, at deep sub-barrier energies, the breakup cross-section accounts for almost the whole total cross-section, where at $E_{\rm c.m.}/V_{\rm B} \leq 0.6$, we obtained $\sigma_{\rm BU}/\sigma_R \simeq 0.92$. It is therefore clear that the enhancement of the breakup cross-section by the continuum–continuum couplings, is one of the factors that can justify the predominance of the breakup channel at deep sub-barrier energies. In our calculation, although the total fusion is negligible compared to the breakup and total reaction cross-sections, it represents about 30 mb. We therefore believe that a total fusion measurement for ^{8}B + ^{208}Pb at 30 MeV and even slightly below can be performed, which could be an important measurement, from an astrophysical perspective, as suggested in ref. [13].

In discussing the enhancement of the breakup cross-section at deep sub-barrier energies ($E_{\rm c.m.}/V_{\rm B} \leq 0.6$) in figure 1, we resorted to the concept of nuclear absorption in the inner region. For this argument to be corroborated at these deep sub-barrier energies, the continuum–continuum couplings need to enhance the breakup cross-section in the inner region. To verify this, we plot in figure 4, the angular momentum distribution cross-sections as a function of the ratio L/K_{α_b}. This ratio represents the radial distance through the classical relation $L = K_{\alpha_b} R$, were K_{α_b} is the wave number in the entrance channel. It is observed in this figure that for $E_{\rm c.m.}/V_{\rm B} \leq 0.6$

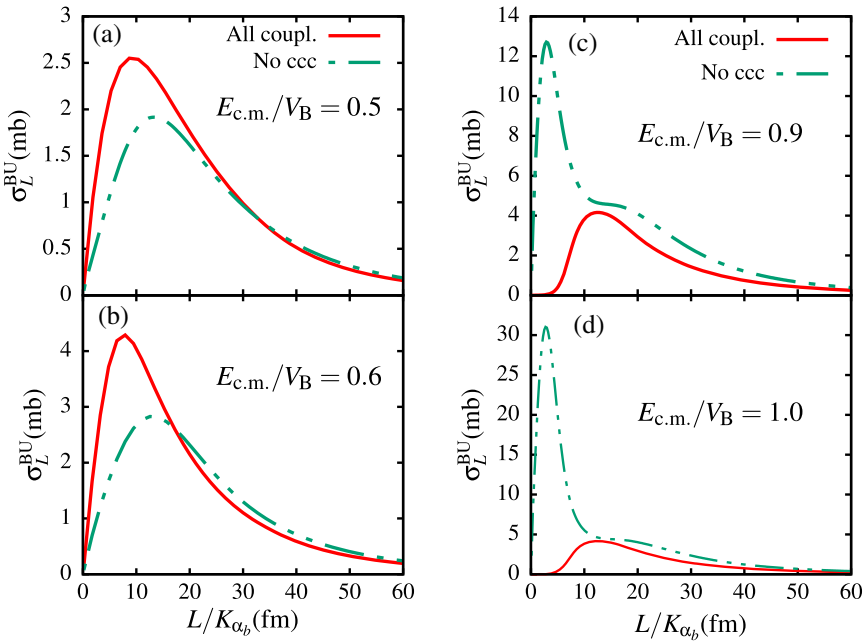

Figure 4. Angular momentum distribution cross-sections as functions of the ratio L/K_{α_b}, in the presence and absence of the continuum–continuum couplings when $\varepsilon_{c.m.}/V_B \leq 1.5$.

(left panels), the breakup cross-section in the presence of the continuum–continuum couplings is more important in the inner region, whereas in the peripheral region, the breakup cross-section in the absence of these couplings seems to prevail. Therefore, this result enforces our conclusion that at deep sub-barrier energies, continuum–continuum couplings enhance the breakup cross-section in the inner region, and among other factors, this can explain the predominance of the breakup channel in the energy range. This result would pave a way towards further investigation of the breakup effect on nuclear astrophysical quantities of interest.

5. Conclusions

In this paper, we have analysed the breakup dynamics at deep sub-barrier energies in the $^{8}B + {}^{208}Pb$ breakup reaction. To this end, we have studied the effect of continuum–continuum couplings on the breakup and complete fusion cross-sections. It is found that at deep sub-barrier energies, the breakup cross-section is enhanced by the inclusion of the continuum–continuum couplings in the coupling matrix elements, and becomes strongly enhanced for a large projectile ground-state binding energy. The analysis of the angular momentum distributions breakup cross-section reveals that this enhancement occurs in the absorption region. We argue that the enhancement of the breakup cross-section due to continuum–continuum couplings may be associated with a projectile breakup on the outgoing trajectory. Although rough, this argument may lead to further investigation in this direction.

Comparing the total reaction, total fusion and breakup cross-sections at deep sub-barrier energies, it is found that the breakup cross-section accounts for about 92% of the total reaction cross-section, thus confirming the conclusion of ref. [13]. We then conclude that the breakup cross-section enhancement at deep sub-barrier energies, as opposed to its suppression at energies above the barrier, can among other factors explain the predominance of the breakup channel at deep sub-barrier energies. Although the total fusion is found to be negligible compared to the breakup and total reaction cross-sections, we believe that a total fusion measurement for $^{8}B+{}^{208}Pb$ at deep sub-barrier energies may be feasible, which could be an import from an astrophysical perspective, as suggested in ref. [13].

We also found that the continuun–continuum couplings strongly enhance the complete fusion cross-section at sub-barrier energies, whereas they suppress it at energies above the barrier. Therefore, we assert that any couplings among continuum states would produce a complete fusion suppression at energies above the barrier, and not only couplings among resonant states, as it has been reported in different works.

In conclusion, the continuum–continuum couplings play a crucial role in the breakup process at deep sub-barrier incident energies. This result may reveal an

important effect of these couplings on nuclear astrophysical quantities of interest. A further study in this direction would be of great interest.

References

[1] I Tanihata *et al*, *Phys. Rev. Lett.* **55**, 2676 (1985)
[2] I Tanihata, H Savajols and R Kanungo, *Prog. Part. Nucl. Phys.* **68**, 21 (2013)
[3] V Jha, V V Parkar and S Kailas, *Phys. Rep.* **845**, 1 (2020)
[4] L F Canto *et al*, *Phys. Rep.* **596**, 1 (2015)
[5] L F Canto *et al*, *Eur. Phys. J. A* **56**, 281 (2020)
[6] B B Back *et al*, *Rev. Mod. Phys.* **86**, 317 (2014)
[7] B Mukeru, M L Lekala and A S Denikin, *Nucl. Phys. A* **935**, 18 (2015)
[8] L F Canto *et al*, *Phys. Rev. C* **80**, 047601 (2009)
[9] J Lubian *et al*, *Phys. Rev. C* **79**, 064605 (2009)
[10] F M Nunes and I J Thompson, *Phys. Rev. C* **57**, R2818 (1998), *Phys. Rev. C* **59**, 2652 (1999)
[11] B Mukeru, G J Rampho and M L Lekala, *J. Phys. G: Nucl. Part. Phys.* **45**, 045101 (2018)
[12] A Pakou *et al*, *Eur. Phys. J. A* **51**, 55 (2015)
[13] A Pakou *et al*, *Phys. Rev. C* **102**, 031601(R) (2020)
[14] C A Bertulani, *Phys. Rev. C* **49**, 2688 (1994)
[15] H Esbensen, G F Bertsch and K A Snover, *Phys. Rev. Lett.* **94**, 042502 (2005)
[16] K J Cook *et al*, *Phys. Rev. C* **97**, 021601(R) (2018)
[17] K J Cook *et al*, *Phys. Rev. Lett.* **122**, 102501 (2019)
[18] K J Cook *et al*, *Phys. Rev. C* **93**, 064604 (2016)
[19] S Kalkal *et al*, *Phys. Rev. C* **93**, 044605 (2016)
[20] E C Simpson *et al*, *Phys. Rev. C* **93**, 024605 (2016)
[21] A G Camacho, A Diaz-Torres and H Q Zhang, *Phys. Rev. C* **99**, 054615 (2019)
[22] A Diaz-Torres and D Quraishi, *Phys. Rev. C* **97**, 024611 (2018)
[23] B Mukeru and M L Lekala, *Phys. Rev. C* **94**, 024602 (2016)
[24] A G Camacho *et al*, *Phys. Rev. C* **91**, 014607 (2015)
[25] J P Fernández-García *et al*, *Phys. Rev. C* **92**, 054602 (2015)
[26] B Mukeru, G J Rampho and M L Lekala, *Nucl. Phys. A* **969**, 60 (2018)
[27] A Diaz-Torres and I J Thompson, *Phys. Rev. C* **65**, 024606 (2002)
[28] B Mukeru, M L Lekala and G J Rampho, *J. Phys. G: Nucl. Part. Phys.* **42**, 085110 (2015)
[29] N Austern *et al*, *Phys. Rep.* **154**, 125 (1987)
[30] Y Iseri *et al*, *Prog. Theor. Phys. Suppl.* **89**, 84 (1986)
[31] L F Canto and M S Hussein, *Scattering theory of molecules, atoms and nuclei* (World Scientific Publishing Co. Pvt. Ltd., Singapore, 2013)
[32] I J Thompson and F M Nunes, *Nuclear reactions for astrophysics* (Cambridge University Press, New York, 2009), See also www.fresco.org.uk
[33] P Descouvemont L F Canto and M S Hussein, *Phys. Rev. C* **95**, 014604 (2017)
[34] K Hagino *et al*, *Phys. Rev. C* **61**, 037602 (2000)
[35] G R Satchler *et al*, *Ann. Phys.* **178**, 110 (1987)
[36] W Wang *et al*, *Chin. Phys. C* **41**, 030003 (2017), See also at https://www.nndc.bnl.gov/nudat2/
[37] H Esbensen and G F Bertsch, *Nucl. Phys. A* **600**, 37 (1996)
[38] J Cook, *Nucl. Phys. A* **388**, 153 (1982)
[39] M Mazzocco *et al*, *Phys. Rev. C* **100**, 024602 (2019)
[40] L C Chamon *et al*, *Phys. Rev. C* **66**, 014610 (2002)